Journal of Alloys and Compounds 509 (2011) 3899–3906

Contents lists available at ScienceDirect

Journal of Alloys and Compounds

journal homepage: www.elsevier.com/locate/jallcom

Charge compensation, electrical and dielectric behavior of lanthanum doped $CaCu_3Ti_4O_{12}$

Ashutosh Kumar Dubey[a,*], Prakash Singh[b], Sindhu Singh[c], Devendra Kumar[c], Om Parkash[c]

[a] School of Materials Science and Technology, Institute of Technology, Banaras Hindu University, Varanasi 221005, India
[b] Department of Ceramic Engineering, CET, Bikaner 334004, Rajasthan, India
[c] Department of Ceramic Engineering, Institute of Technology, Banaras Hindu University, Varanasi 221005, India

ARTICLE INFO

Article history:
Received 4 August 2010
Received in revised form
19 December 2010
Accepted 21 December 2010
Available online 28 December 2010

Keywords:
$CaCu_3Ti_4O_{12}$
Charge compensation
ac conductivity
dc conductivity

ABSTRACT

Mechanism of charge compensation on lanthanum, (La^{3+}) substitution on Ca site in calcium copper titanate ($CaCu_3Ti_4O_{12}$), and its effect on resulting electrical and dielectric properties has been studied in the present investigation. For this purpose samples were prepared according to two stoichiometries viz. $La_xCa_{(1-3x/2)}Cu_3Ti_4O_{12}$ ($x \leq 0.09$) and $La_xCa_{(1-x)}Cu_3Ti_4O_{12}$ ($x = 0.03$) by solid state ceramic route. The former represents ionic compensation while the later is in accordance with electronic compensation. Nature of charge carriers is identified by measuring Seebeck coefficient which is found to be negative in the entire range of measurement. In order to understand the mechanism of conduction, ac conductivity is measured as a function of temperature and frequency. Space charge polarization is the dominant polarization mechanism phenomenon at low frequency and high temperature while orientation polarization dominates at low temperature and high frequency. Impedance analysis confirms the formation of internal barrier layers which is responsible for high dielectric constant in these samples.

1. Introduction

Giant, static dielectric constant ($\sim 10^4$) exhibited by pseudoperovskite $CaCu_3Ti_4O_{12}$ (CCTO) can make it important for many applications in microelectronics and memory devices. Its dielectric constant remains almost unchanged between 100 and 500 K in the frequency range 10^2–10^6 Hz [1–3]. At temperature below 100 K, the dielectric constant drop rapidly to around 100 without any structural phase transition [2]. In order to explain the giant dielectric constant, several models have been proposed [2,3]. Sinclair et al. [2] demonstrated that $CaCu_3Ti_4O_{12}$ is electrically heterogeneous with semiconducting grains and insulating grain boundaries, which forms internal barrier layer capacitor (IBLC). Subramanian et al. [4] have suggested that the unusual crystal structure of $CaCu_3Ti_4O_{12}$ ceramics may be responsible for high dielectric permittivity.

In a study by Ramiez et al. [5], it was speculated that the collective ordering of local dipole moments may be one of the possible reasons for its high permittivity value. In a single crystal, spatial inhomogeneity of local dielectric response can give rise to giant dielectric constant [3]. Lunkenheimer et al. [6] shown that the high permittivity in $CaCu_3Ti_4O_{12}$ is due to contact-electrode depletion effect.

To date, the internal barrier layer capacitor (IBLC) formation explanation of giant permittivity value is comparatively widely accepted [1]. Although, CCTO possesses giant dielectric constant, the dielectric losses are too high to commercialize it. Number of attempts has been made to decease tan δ by various compositional modifications such as Cr_2O_3-doped CCTO [7], ZrO_2-doped CCTO [8], CCTO/$CaTiO_3$ composite [9], B_2O_3 doped CCTO [10], TiO_2-rich CCTO [11,12] and La substitution on Cu sites in CCTO [13] have been reported to be effective in reducing the dielectric loss and still maintaining high dielectric constant. In a study by Cheng et al. [14], it was shown that in La doped $CaCu_3Ti_4O_{12}$, Ca site is completely substituted by La without influencing the phase transition. In addition, they reported that the grain size of CCTO ceramic can be controlled by La content and consequently the electric properties of IBLC [14].

Most of these studies were intended to minimize the loss by controlling mainly the grain boundary chemistry.

In the present investigation, Ca^{2+} is partially substituted by La^{3+} ion in the system according to two stoichiometries $La_xCa_{(1-3x/2)}Cu_3Ti_4O_{12}$ ($x = 0.01, 0.03, 0.05, 0.07, 0.09$) and $La_xCa_{(1-x)}Cu_3Ti_4O_{12}$ ($x = 0.03$) under optimum sintering conditions. In the first system, the charge neutrality is maintained by ionic compensation and in the later, the charge neutrality is maintained by electronic compensation mechanism. Most appropriate mechanism of charge compensation on substitution of La on Ca site and its effect on resulting dielectric and electrical

* Corresponding author. Present address: Laboratory for Biomaterials, Department of Materials Science and Engineering, Indian Institute of Technology, Kanpur 208016, India. Tel.: +91 512 2597920.
E-mail address: akdubey@iitk.ac.in (A.K. Dubey).

0925-8388/$ – see front matter © 2010 Elsevier B.V. All rights reserved.
doi:10.1016/j.jallcom.2010.12.156

properties has been studied. The nature of charge carriers and mechanism of conduction have also been discussed. Impedance analysis has been carried out to separate out the contribution of grains (bulk) and grainboundaries to the total observed resistance and capacitance in order to understand their electrical behavior. Electrical conductivity and dielectric properties are studied on the same materials in order to correlate these two behaviors.

2. Experimental

$Ca_{1-x}La_xTi_3Cu_4O_{12}$ ($x = 0.03$) and $Ca_{(1-3x/2)}La_xCu_3Ti_4O_{12}$ with $x = 0.01, 0.03, 0.05, 0.07$ and 0.09 have been synthesized by solid state ceramic route as indicated by Eqs. (1) and (2) respectively.

$$La_2O_3 + 9CuO + 12TiO_2 \xrightarrow{3CaO} 2(La_{Ca^{2+}}{}^{3+})^{\bullet} + 9(Cu_{Cu^{2+}}{}^{2+})^{*} + 12(Ti_{Ti^{4+}}{}^{4+})^{*} + 36O_O + V_{Ca}'' \quad (1)$$

$$La_2O_3 + 6CuO + 8TiO_2 \xrightarrow{2CaO} 2(La_{Ca^{2+}}{}^{3+})^{\bullet} + 6(Cu_{Cu^{2+}}{}^{2+})^{*} + 8(Ti_{Ti^{4+}}{}^{4+})^{*} + 25O_O + 2e' \quad (2)$$

where, all the species are written according to the Kroger-Vink notation of defects.

Appropriate amounts of $CaCO_3$, CuO, TiO_2 and lanthanum oxalate of purity ≥99% for all the above mentioned compositions were weighed and mixed in a ball mill using agate as grinding media and acetone as a mixing medium for 7 h in agate jars. Mixed powders were dried overnight in the oven. Dried powders were calcined at 1273 K for 12 h in a platinum crucible. Calcined powder was compacted under an optimum load of 70 KN in the form of cylindrical discs (dia. ~12 mm) using 2% solution of PVA as binder. The pellets were slowly heated to 773 K and then held at this temperature for an hour to burn off the binder. Thereafter the temperature was raised to 1348 K and the pellets were sintered in air at this temperature for 20 h and furnace cooled. The sintered pellets were grind and powder X-ray diffraction patterns were recorded using a 12 kW rotating anode (Cu) based Rigaku powder diffractometer operating in the Bragg–Brentano geometry and fitted with a graphite monochromator in the diffracted beam employing Cu-$K_{\alpha 1}$ radiation with a Ni filter. The bulk density was calculated using Archimedes Principle. Percentage porosity was determined using theoretical and experimental density. Seebeck coefficient was measured in the temperature range (600–1000 K) in air on thick pellets of thickness ~7 mm. Escort EDM 3150 Multimeter was used to measure voltage. For DC resistivity and dielectric measurements, the samples were polished and electroded using Ag-Pd alloy paint which was cured by heating at 1073 K for 20 min. The resistance was measured by two probe method in the temperature range 300–1000 K using Keithley 616 Electrometer at steady temperatures.

Capacitance, C, dielectric loss, D and AC conductance, G were measured in the frequency range 100 Hz to 1 MHz at a few selected steady temperatures in the range 300–525 K in a locally fabricated cell using programmed HIOKI 3552-50 LCR Hi-Tester.

AC conductivity was calculated by the relationship:

$$\sigma_{ac} = \frac{G \times d}{A} (\text{ohm cm})^{-1} \quad (3)$$

where σ_{ac} is the AC conductivity, d is the thickness (in cm), G is the conductance in ohm^{-1} and A is the area (in cm^2) of the sample. The value of real and imaginary part of impedance i.e. Z' and Z'' were calculated using the formula:

$$Z' = \frac{1}{[G(1 + (1/D^2))]} \quad (4)$$

and

$$Z'' = \frac{Z'}{D} \quad (5)$$

3. Results and discussion

3.1. Crystal structure

Powder X-ray diffraction (XRD) patterns for various compositions in the system $La_xCa_{1-3x/2}Cu_3Ti_4O_{12}$ ($x = 0.00, 0.01, 0.03, 0.05, 0.07, 0.09$) and $La_xCa_{1-x}Cu_3Ti_4O_{12}$ ($x = 0.03$) prepared by solid state ceramic route are shown in Fig. 1. Formation of single phase was confirmed by absence of the characteristic lines of constituent oxides or the other phases in the powder X-ray diffraction patterns of the system $La_xCa_{1-3x/2}Cu_3Ti_4O_{12}$, whereas for the sample $La_xCa_{1-x}Cu_3Ti_4O_{12}$ single phase did not form (Fig. 1(b)). This indi-

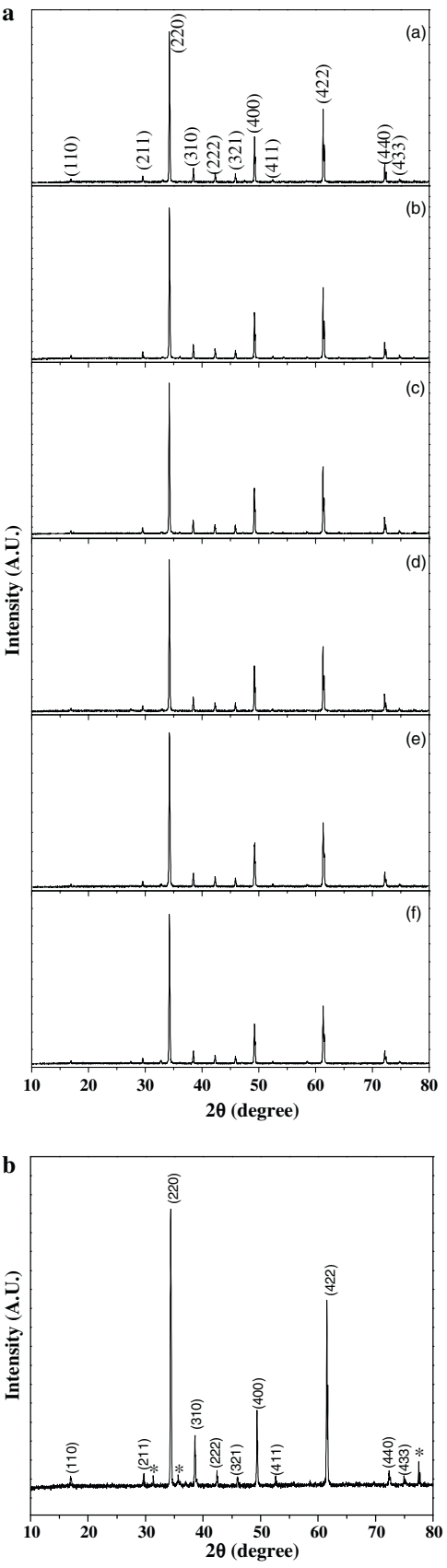

Fig. 1. (a) X-ray diffraction pattern of compositions in the system $La_xCa_{(1-3x/2)}Cu_3Ti_4O_{12}$ for (a) $x = 0.00$, (b) $x = 0.01$, (c) $x = 0.03$, (d) $x = 0.05$, (e) $x = 0.07$ and (f) $x = 0.09$. (b) X-ray diffraction pattern of composition $x = 0.03$ in the system $Ca_{(1-x)}La_xCu_3Ti_4O_{12}$. * shows the impurity phases.

Table 1
Lattice parameter and % porosity of various compositions prepared in the system $La_xCa_{(1-3x/2)}Cu_3Ti_4O_{12}$.

Composition	Lattice parameter (Å)	% porosity
$x = 0.00$	7.392	9.07
$x = 0.01$	7.393	8.36
$x = 0.03$	7.399	7.35
$x = 0.05$	7.396	6.99
$x = 0.07$	7.398	6.01
$x = 0.09$	7.398	6.22

cates that the charge neutrality in the system is maintained via ionic compensation mechanism in these materials.

Powder X-ray diffraction (XRD) data for all the single phase compositions could be indexed on the basis of a cubic unit cell similar to $CaCu_3Ti_4O_{12}$. Lattice parameters, crystal structure, theoretical density, experimental density and percentage porosity for all the compositions are given in Table 1. Lattice parameter increases slightly with increase in La content. This is due to larger ionic radii of La^{3+} as compared to Ca^{2+}. It was found that bulk density for various samples was greater than 90% of theoretical value. Percentage porosity decreases (i.e. sinterability increases) with increasing x.

3.2. Seebeck-coefficient

Plots of Seebeck co-efficient, α vs. temperature in the temperature range 450–1000 K for all the compositions are shown in Fig. 2. Below 450 K, the measurement of Seebeck coefficient is not reliable because of high resistance of the samples. The negative value of α over the entire temperature range of measurement indicates that the electrons are the majority charge carriers. Value of α decreases with increase of temperature (becomes more negative) and it is small for all the samples.

Plots of logarithm of DC resistivity, $\log \rho_{dc}$ (ohm-cm) vs. $1000/T$ (K^{-1}) are shown in Fig. 3. For all the compositions resistivity decreases with increasing temperature. These plots are found to have a linear region in a certain temperature range. This shows that resistivity in these regions obey Arrhenius equation:

$$\rho_{dc} = \rho_0 \exp\left(\frac{E_a}{kT}\right) \quad (6)$$

where E_a, is the activation energy for conduction and k is the Boltzmann constant. Values of activation energies obtained by least square fitting of the resistivity data for various compositions are

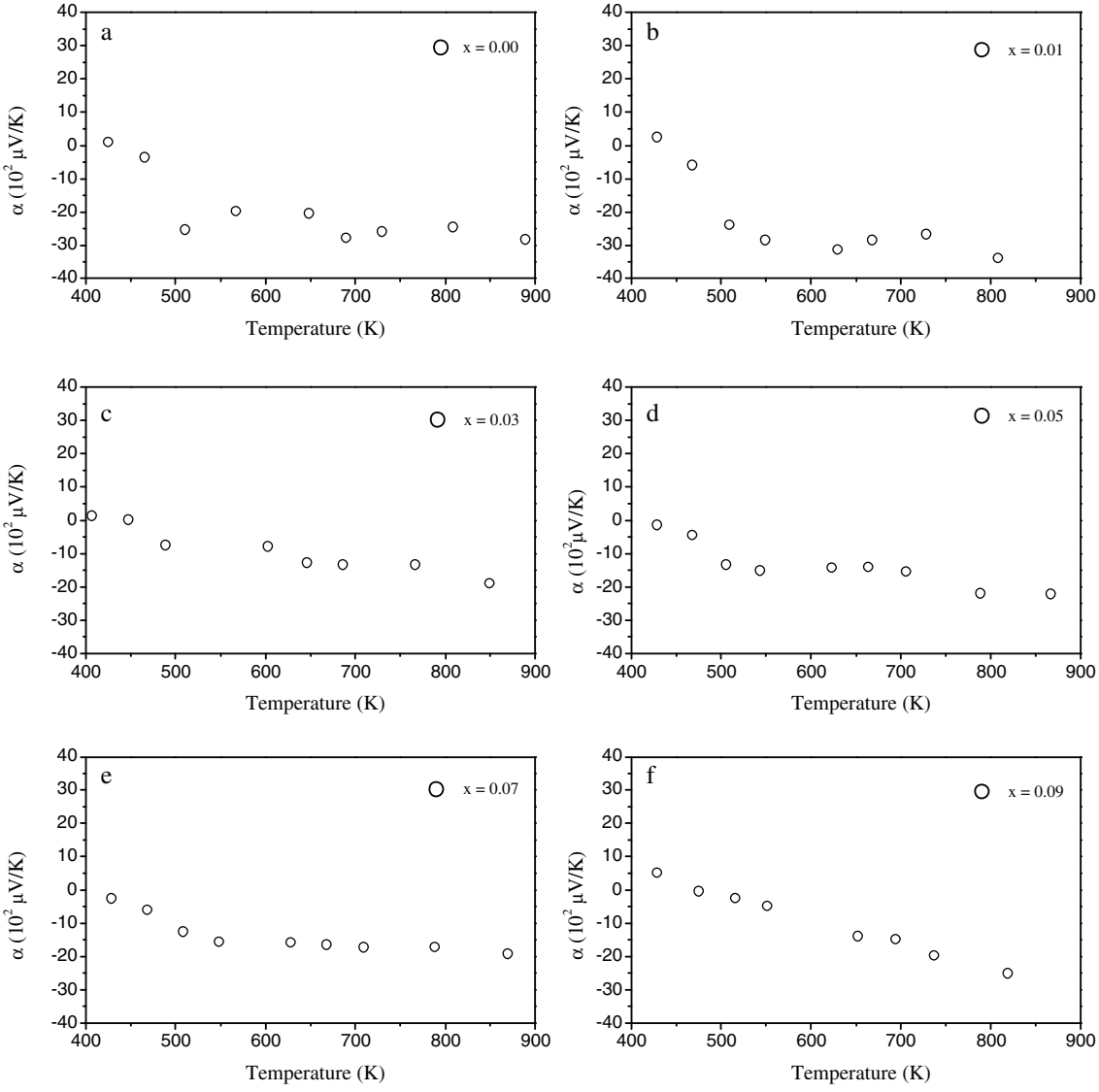

Fig. 2. Variation of Seebeck coefficient, α with temperature for various compositions in the system $La_xCa_{(1-3x/2)}Cu_3Ti_4O_{12}$.

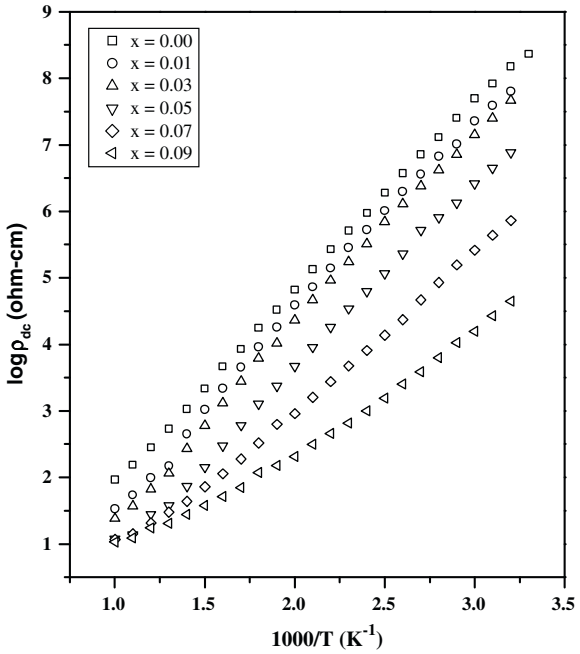

Fig. 3. Variation of log ρ_{dc} with inverse of temperature for the various samples in the system $La_xCa_{(1-3x/2)}Cu_3Ti_4O_{12}$.

given in Table 2. Values of activation energies for these samples lie in the range 0.36–0.59 eV.

3.3. AC conductivity behavior

Variation of log σ_{ac} with log f at a few selected temperatures for a typical composition $x = 0.09$ is shown in Fig. 4(a). For composition with $x = 0.09$, there are two plateaus and two dispersion regions observed up to 400 K while one plateau and one dispersion region is observed at 450 K and 500 K. For all the compositions, it is found that a plateau is observed in the low frequency region followed by a frequency dispersion region. The transition between these regions shifts to higher frequency with increasing temperature. Therefore, high frequency dispersive region disappears at 500 K. At 500 K, only one plateau region is observed over the entire frequency range. The plateaus appearing in the low frequency region at $T \leq 450$ K represent the total conductivity of the grains and grain boundaries while the other plateau represents the contribution of only grains to the total conductivity observed at various temperatures.

log σ_{ac} vs. 1000/T plot (Fig. 4(a)) shows very small temperature dependence but strong frequency dependence at low temperatures. A weak frequency dependence and strong temperature dependence is observed at high temperatures. In the high temperature region a higher slope and very little frequency dependence is seen. In the high temperature region, the variation of log σ_{ac} with inverse of temperature is linear. AC conductivity in this region follows the relation $\sigma = \sigma_0 \exp(-E_a'/kT)$, where E_a' is the activation energy for AC conduction. Here $E_a' = E_a + E_H$, where E_H is the hoping energy and E_a is activation energy for DC conduction [21].

Table 2
The activation energies, E_a for different compositions in the system $La_xCa_{(1-3x/2)}Cu_3Ti_4O_{12}$.

Compositions (x)	Temperature range (K)	Activation energy (DC) (eV)
$x = 0.00$	300–1000 K	0.57 ± 0.01
$x = 0.01$	310–830 K	0.58 ± 0.01
$x = 0.03$	310–710 K	0.57 ± 0.03
$x = 0.05$	310–710 K	0.56 ± 0.02
$x = 0.07$	310–670 K	0.47 ± 0.02
$x = 0.09$	310–625 K	0.36 ± 0.03

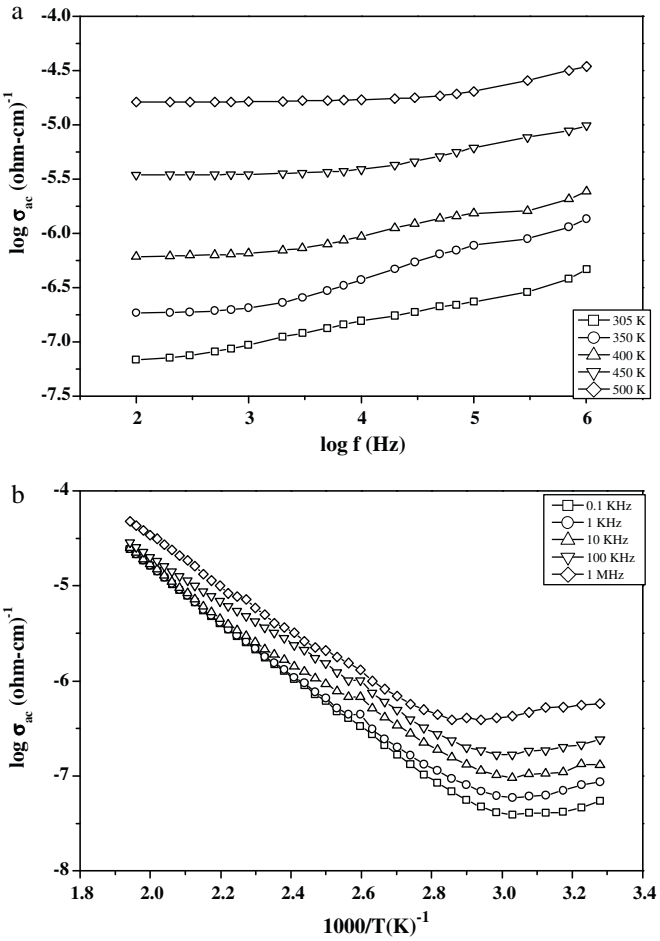

Fig. 4. Variation of log σ_{ac} with (a) log frequency and (b) inverse of temperature for the composition $x = 0.09$ in the system $La_xCa_{(1-3x/2)}Cu_3Ti_4O_{12}$.

It has been reported that these titanates, lose traces of oxygen during their sintering at high temperature, depending on the thermodynamic conditions, leading to formation of oxygen vacancies [15,16],

$$O_O^* \Leftrightarrow V_O^{\bullet\bullet} + 2e' + \frac{1}{2}O_2 \quad (7)$$

Here, all the species are written according to Kronger-Vink notation of defects.

At temperatures above 1275 K, oxygen vacancies are doubly ionized, $V_O^{\bullet\bullet}$. At temperatures below 675 K, these oxygen vacancies turn into singly ionized $V_O^{\bullet}$ [17]. The change on ionization can be written as [17,18]:

$$V_O^{\bullet\bullet} + e' \Leftrightarrow V_O^{\bullet} \quad (8)$$

Also, the doubly ionized oxygen vacancies are frozen in the sample at or near room temperature because enough time is not given to the sample to equilibrate with the surrounding oxygen. Hence, both singly and doubly ionized oxygen vacancies coexist at or near room temperature. The concentration of $V_O^{\bullet\bullet}$ increases and concentration of $V_O^{\bullet}$ decreases with increase in temperature. Electron released in relation (7) imparts n-type semiconductor behavior to these materials.

Electron released in the reaction (7) may be captured by Ti^{4+} or Cu^{2+} to form Ti^{3+} and Cu^{+}, respectively. Cu^{+} with electronic configuration $3d^{10}$ is stable while Ti^{3+} with $3d^1$ configuration is unstable.

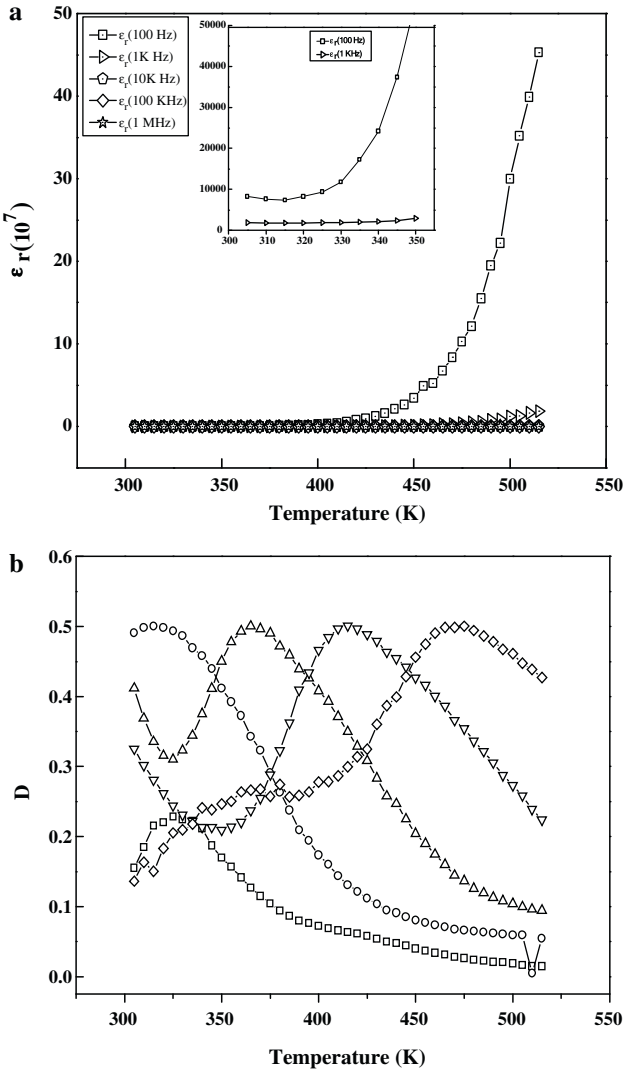

Fig. 5. Variation of (a) dielectric constant, ε_r and (b) dielectric loss, D with temperature at a few selected frequencies for composition $x = 0.05$ in the system $La_xCa_{(1-3x/2)}Cu_3Ti_4O_{12}$.

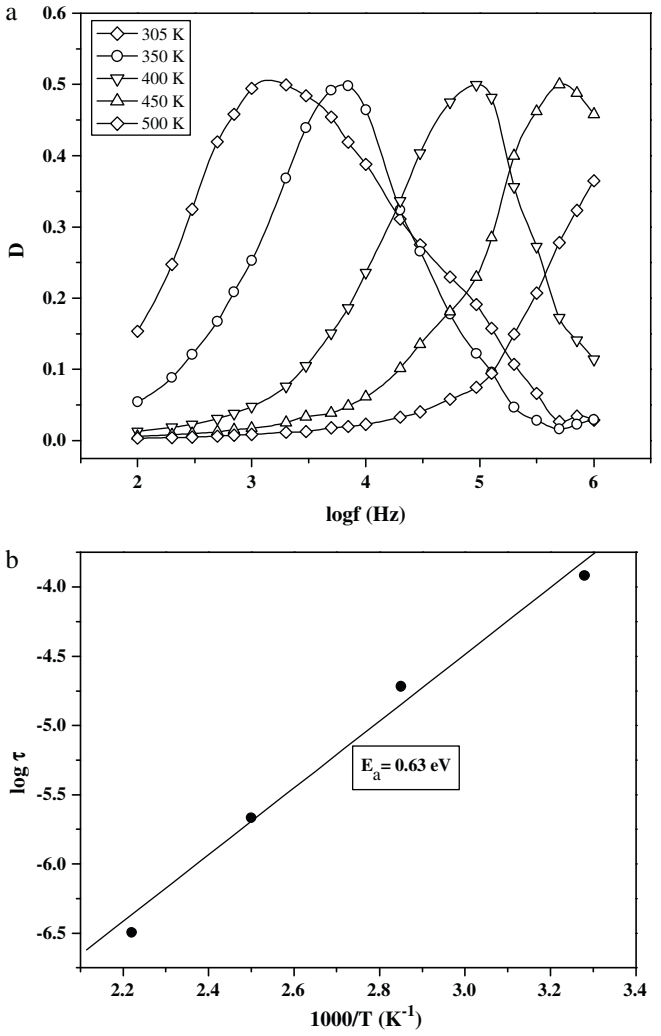

Fig. 6. (a) Variation of (a) ε_r and (b) D with log frequency at a few steady temperatures for composition $x = 0.03$ in the system $La_xCa_{(1-3x/2)}Cu_3Ti_4O_{12}$. (b) Variation of log τ with inverse of temperature for composition $x = 0.03$ in the system $La_xCa_{(1-3x/2)}Cu_3Ti_4O_{12}$.

Therefore, the probability of formation of Cu^+ is more as compared to Ti^{3+}. Cu^+ on Cu^{2+} site carries effective negative charge $(Cu^{+}_{Cu^{2+}})'$. These materials, therefore, contain defects such as $La_{Ca}^{\bullet}$, V_{Ca}'', $V_O^{\bullet}$, $V_O^{\bullet\bullet}$ and $(Cu^{+}_{Cu^{2+}})'$. At low temperature (near room temperature) due to Coulombic interaction, positively charged defects attract negatively charged defects. This leads the formation of associated defects pairs such as $(Cu_{Cu^{2+}}{}^{+})'$–$V_O^{\bullet\bullet}$, V_{Ca}''–$2V_O^{\bullet}$ or V_{Ca}''–$2(La_{Ca}^{\bullet})$ [19]. Hopping of electrons among copper ions of various valencies or of O^{2-} ions around Cu^+/Cu^{++} or Ti^{4+} through vacant oxygen sites, $V_O^{\bullet\bullet}$ will lead to the rotation of dipoles [19]. In the low temperature region, frequency dependent and temperature independent ac conductivity is observed because the hoping of charge carriers will lead to the rotation of dipoles [19,20]. In other words, we can say that metal ion-oxygen vacancy complexes give rise to the defect states in the forbidden band gap. At low temperatures, the hoping among these defects states give rise to orientation of dipoles and AC electrical conductivity will be frequency dependent and less dependent on temperature [20]. With increase in temperature, these pairs of defects dissociate giving rise to free defect centres. Hopping of electrons among these defects, Cu^+ and Cu^{++} will contribute to the long range migration of charge carriers i.e., excitation of charge carriers at conduction band edge and hoping at energies close to it, which leads to n-type conduction [19]. In this case, AC electrical conductivity is almost independent of frequency and exponentially dependent on temperature as expected [20]. Value of W_H, calculated for the composition $x = 0.09$ from the difference in E_a' and E_a, is 0.15 eV which is of right magnitude for hoping of electrons

3.4. Dielectric behavior

Plots of ε_r and D vs temperature at a few selected frequencies and ε_r and D vs log f at a few steady temperatures for a typical composition $x = 0.07$ are shown in Fig. 5. Behavior of other compositions are similar. It is observed that in the permittivity ε_r vs. T plots, at room temperature the value of dielectric constant is of the order of 10^4 at 100 Hz for all the compositions. Value of permittivity is nearly constant in the temperature range 300–450 K for all the compositions. With increase in frequency, the temperature beyond which dielectric constant increases shift toward higher temperature side. The increase in the value of ε_r is more pronounced with increase in temperature at lower frequencies.

D vs. T plots for all the compositions show one or two peaks for these materials which are due to the relaxation processes in these materials. With increase in frequency, the positions of the peaks shift toward the higher temperature side.

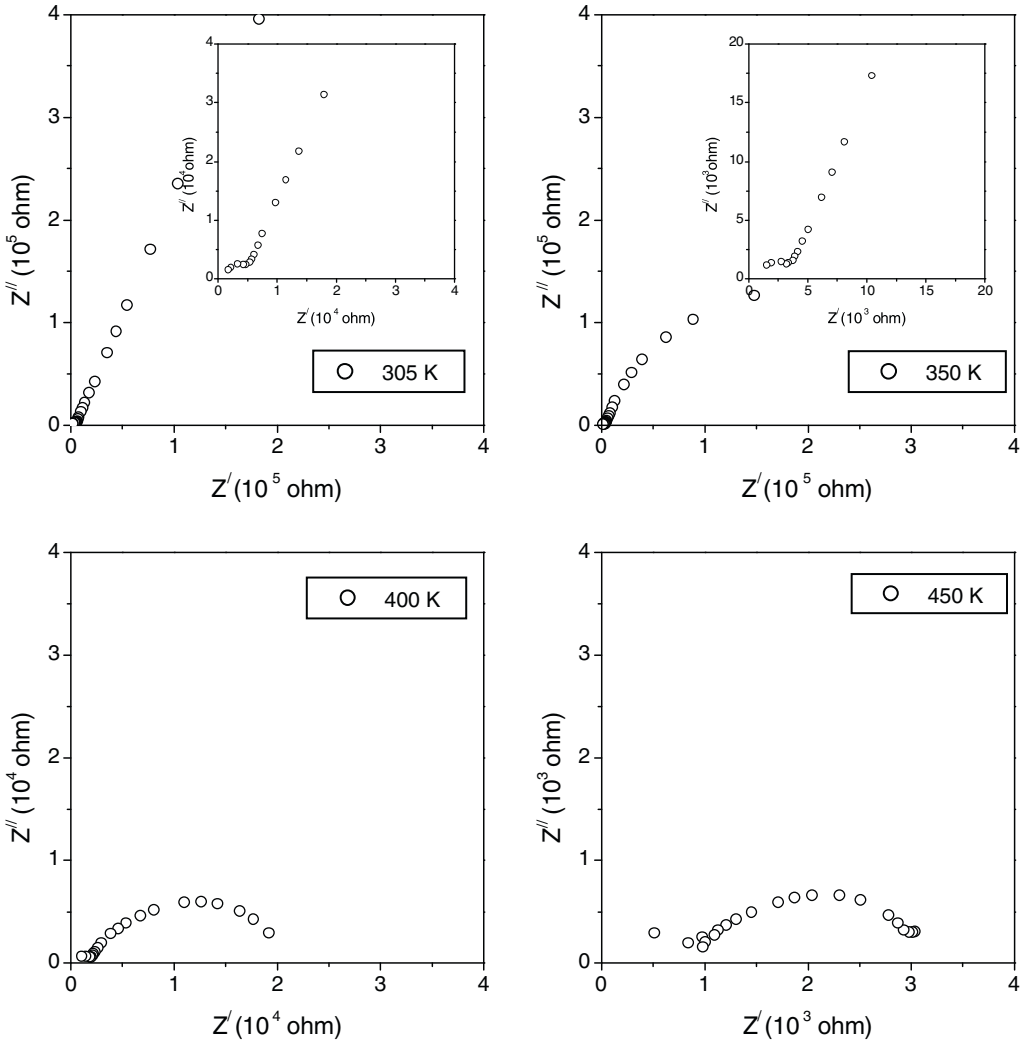

Fig. 7. Complex plane impedance (Z'' and Z') plots at different temperatures for $x = 0.01$ in the system $Ca_{(1-3x/2)}La_xCu_3Ti_4O_{12}$.

From the variation of dielectric constant with temperature and frequency, it can be concluded that the dielectric behavior of these materials at lower frequencies is predominantly due to space charge polarization. The space charge polarization arises due to the presence of two or more phases with different electrical conductivity are present in the sample. The grains (semiconducting) and grain boundaries (insulating) have different electrical conductivities (as shown by results of impedance analysis discussed later). With increase in temperature this difference increases, which in turn gives rise to more contribution of space charge polarization and hence there is abrupt increase in dielectric constant at low frequencies.

The peaks observed in the low frequency region in D vs. $\log f$ (Fig. 6(a)) plots is due the relaxation of the space charge polarization, which shifts toward higher frequency side with increase in temperature. The second peak in high frequency side shows the relaxation of dipolar polarization. The formation of associated defect pairs has already been described earlier. The value of activation energy for conduction, calculated from Fig. 6(b), is 0.63 eV. This value matches with the activation energy for dc conduction.

3.5. Impedance analysis

Complex plane impedance (Z'' vs Z') plots for the composition with $x = 0.01$ at a few selected temperatures are shown in Fig. 7. From these plots it is observed that at all temperatures two depressed circular arcs are found. The smaller arc in the high frequency region (near origin) represents the contribution of grains while the arc in the lower frequency range (away from origin) represents the contribution of grain boundaries [21]. Values of R_g and R_{gb} can be obtained from the intercepts of these arcs of Z'' vs. Z' plots with Z' axis. Intercept of high frequency arc passing through origin gives values of R_g and intercept of arc with low frequency range gives the contribution of grainboundaries.

Each semicircular or depressed arc in the complex plane plots represents a particular relaxation process. A semicircular arc having origin on the real axis shows a single relaxation process, while the depressed arc shows that there is either more than one relaxation process or there is one process in which there is distribution of relaxation times [21]. In the samples under investigation, the depressed arcs are found for all the compositions. This result infers that there is distribution of relaxation times. The calculated values of resistance and capacitance due to bulk and grain boundary contributions from complex plane impedance plot for the composition $x = 0.01$ is shown in Table 3. The value of activation energy is calculated from the slope of the curve $\log R_g$ and $\log R_{gb}$ vs. $1000/T$ (Fig. 8). Activation energy, E_a for the grains and grain boundaries is found to be 0.14 eV and 0.59 eV, respectively. This is expected as the overall resistance is due to grainboundaries which form the continuous phase. Therefore, activation energy for

Table 3
Resistance and capacitance values for both bulk and grain boundary contribution determined from complex plane modulus plots $x = 0.01$ in the system $La_xCa_{(1-3x/2)}Cu_3Ti_4O_{12}$.

Temperature (K)	Bulk		Grain boundary	
	R_g (ohm)	C (pF)	R_gb (ohm)	C (nF)
305	6.00×10^3	53.1	–	–
350	3.00×10^3	75.8	1.90×10^5	8.38
400	1.70×10^3	93.7	2.10×10^4	10.80
450	9.47×10^2	245	2.45×10^3	13.00

conduction will be same as for grainboundaries. This is what observed experimentally.

Results show that the resistance and capacitance of the grain boundaries are much more than that of the grains. The resistance of the grain boundaries is found to be three orders of magnitude higher than that of grains, which confirms the formation of barrier layers across the grain boundaries [21]. Values of capacitance obtained for grain and grainboundaries given in Table 3 are point out that these arcs are due to grain and grainboundaries. In order to find out whether conduction is of localized type or occurs due to long range of migrations of charge carriers, both Z'' and M'' are plotted in the same plot as a function of logarithm of measuring frequency, f. If conduction is localized i.e. occurs due to short range movement of the charge carriers, then peak in Z'' and M'' occur at the different frequencies and vice versa for long range movement of charge carriers [22]. Plots of Z'' and M'' vs. log f for the composition $x = 0.03$ at 305 K and 350 K are given in Fig. 9(a) and (b) respectively. Peaks in Z'' and M'' occur at different frequency at 305 K while there are at the same frequency at 350 K. Therefore at low temperature (305 K) conduction occurs due to short range movement of charge carriers while at 350 K it occurs due to long range migration of charge carriers i.e. due to hoping of electrons among Cu^+ and Cu^{++} sites. This is in conformity with the conclusion drawn from the results of AC conductivity as a function of temperature at different frequencies (Fig. 4(b)).

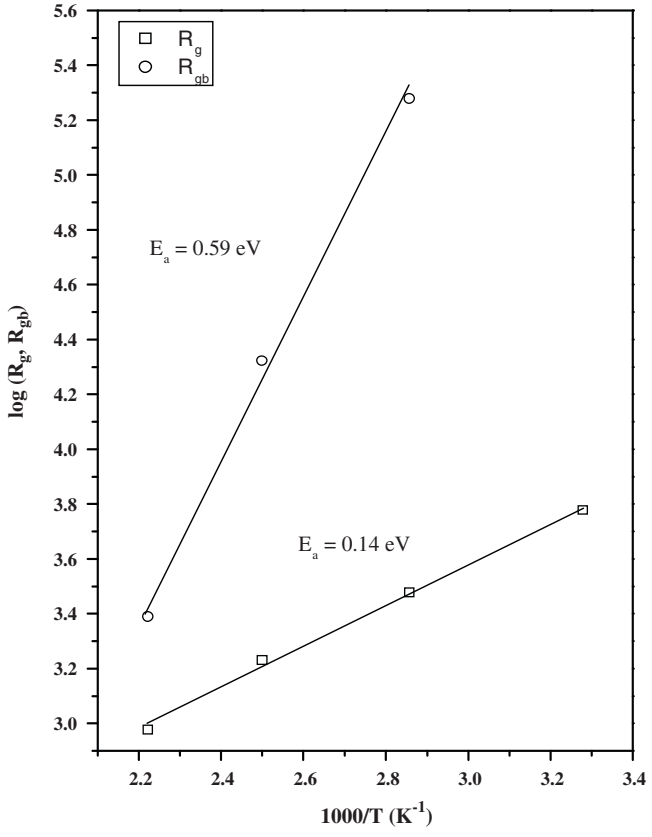

Fig. 8. Variation of log of R with inverse of temperature for $x = 0.01$ in the system $Ca_{(1-3x/2)}La_xCu_3Ti_4O_{12}$.

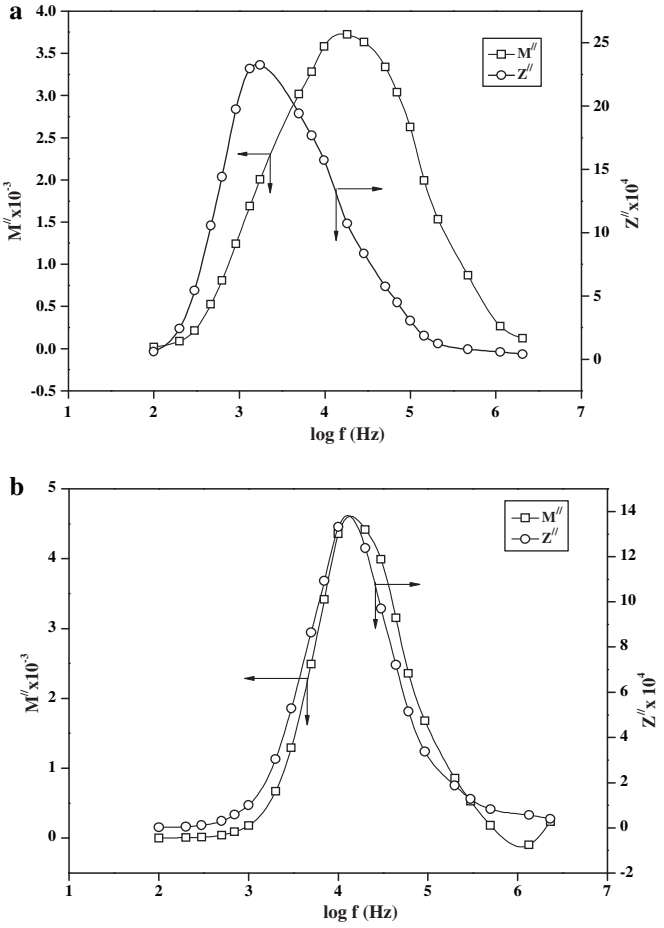

Fig. 9. (a) Variation of (a) Z with log frequency at temperature 305 K for composition $x = 0.03$ in the system $La_xCa_{(1-3x/2)}Cu_3Ti_4O_{12}$. (b) Variation of (a) Z with log frequency at temperature 350 K for composition $x = 0.03$ in the system $La_xCa_{(1-3x/2)}Cu_3Ti_4O_{12}$.

4. Conclusions

Substitution of La^{3+} at Ca^{2+} site, the charge compensation is ionic in nature, i.e. occurs due to vacancies in Ca-sublattice. All the compositions have cubic structure. The negative value of Seebeck coefficient showed that the electrons are the majority charge carriers. Resistivity decreases with temperature indicating semiconducting behavior. Complex plane impedance plots show that the barrier layer formation at grain-grain boundary interface is responsible for the high dielectric constant in these samples. At low temperature, the dipoles are formed in the material due to the presence of defect. Rotation of these dipoles occurs either due to the hoping of oxygen ions into vacant oxygen sites or electrons among Cu^+ and Cu^{2+} sites giving rise to orientational polarization. Space charge polarization dominates at low frequency and high temperature while orientational polarization occurs at low temperature and high frequency. At low temperature conductions occurs due to short range movement and at high temperature occurs due to long range movement of charge carriers.

Acknowledgement

Thanks are due to Dept. of Science and Technology, New Delhi for financial support.

References

[1] M.A. Subramanian, A.W. Sleight, Solid State Sci. 4 (2002) 347.
[2] D.C. Sinclair, T.B. Adams, F.D. Morrison, A.R. West, Appl. Phys. Lett. 80 (2002) 12.
[3] M.H. Cohen, J.B. Neaton, L. He, D. Vanderbilt, J. Appl. Phys. 94 (2003) 3299.
[4] M.A. Subramanian, L. Dong, N. Duan, B.A. Reisner, A.W. Sleight, J. Solid State Chem. 151 (2000) 323.
[5] A.P. Ramiez, M.A. Subramanian, M. Gardel, G. Blumberg, D.L.T. Vogtand, S.M. Shapiro, Solid State Commun. 115 (2000) 217.
[6] P. Lunkenheimer, R. Fichtl, S.G. Ebbinghaus, A. Loidl, Phys. Rev. B 70 (2004) 172102.
[7] S. Kwon, C.C. Huang, E.A. Patterson, Mater. Lett. 62 (2008) 633.
[8] E.A. Patterson, S. Kwon, C.C. Huang, D.P. Cann, Appl. Phys. Lett. 87 (2005) 182911.
[9] Y.Y. Yan, L. Jin, L.X. Feng, G.H. Cao, Mater. Sci. Eng. B 130 (2006) 146.
[10] R. Mazumder, A. Seal, A. Sen, H.S. Maiti, Ferroelectrics 326 (2005) 103.
[11] Y.H. Lin, J. Cai, M. Li, C.W. Nan, J. He, Appl. Phys. Lett. 88 (2006) 172902.
[12] Y.H. Lin, J. Cai, M. Li, C.W. Nan, He, J. Appl. Phys. 103 (2008) 074111.
[13] S. Shao, J. Zhang, P. Zheng, C. Wang, J. Li, M. Zhao, Appl. Phys. Lett. 91 (2007) 042905.
[14] B. Cheng, Y.H. Lin, J. Yuan, J. Cai, C.W. Nan, X. Xiao, J. He, J. Appl. Phys. 106 (2009) 034111.
[15] I. Burn, S. Neirman, Mater. Sci. 17 (1982) 3510.
[16] S. Neirman, I. Burn, J. Mater. Sci. 19 (1984) 737.
[17] R. Moos, K.H. Menesklou, Hardtl, Appl. Phys. A 61 (1995) 389.
[18] R. Moos, K.H. Hardtl, J. Appl. Phys. 80 (1996) 393.
[19] O. Parkash, D. Kumar, A. Goyal, A. Agrawal, A. Mukherjee, S. Singh, P. Singh, J. Phys. D: Appl. Phys. 41 (2008) 035401.
[20] N.F. Mott, E.S. Davis, Electronic Processes in Non-Crystalline Materials, Clarenden, London, 1979 (Chapter 6).
[21] I.M. Hodge, M.D. Ingram, A.R. West, J. Electroanal. Chem. 74 (1996) 125.
[22] R. Gerhardt, J. Phys. Chem. Solids 55 (1994) 1491.